# LARGE EDDY SIMULATIONS OF TRANSIENT TURBULENT FLOW DURING CONTINUOUS SLAB CASTING OF STEEL

**Quan Yuan, S. P. Vanka and Brian G. Thomas**
Mechanical and Industrial Engineering Department
University of Illinois at Urbana-Champaign
Urbana, IL, 61801, USA
quanyuan@uiuc.edu, s-vanka@uiuc.edu, bgthomas@uiuc.edu
Tel.: +1- (217) 244- 2859, +1-(217) 244-8388, +1 – (217) 333- 6919

## ABSTRACT

Three LES computations are presented which simulate the turbulent flow in the liquid-pool during continuous casting of steel. LES is first compared with PIV measurements on a 0.4-scale water model to gauge the accuracy. It is then applied to a steel caster and its corresponding water model. The velocity fields in the liquid-pool are quantified with instantaneous, mean and *rms* values. Transient asymmetries are found both across the top surface and in the lower recirculation zone between the left and right halves, which is an important feature of this flow. Interaction between the two halves is found to be an important cause of the asymmetries. Half-pool simulations inherently miss the asymmetry and the consequent oscillations. This work also quantifies the difference between flow in the steel caster and constructed water models of the process. Finally the top surface liquid level and its fluctuations are predicted and compared with plant data.

## INTRODUCTION

Continuous casting of steel involves complex turbulent flow, which plays an important role in the steel quality. During the continuous casting process, shown in Fig. 1(a), molten steel is directed into the mold cavity by the bifurcated or trifurcated complex geometry SEN (submerged entry nozzle) ports with Reynolds number ~$10^5$. In the liquid-pool the superheat is extracted by the water-cooled tapered mold to form a growing solid shell, which is withdrawn from the mold bottom at the casting speed. Inside the shell, the molten steel flows chaotically in the liquid-pool. Plant observations suggest that flow transients are responsible for intermittent defects. Insights into the transient flow in the liquid-pool are an essential step towards understanding defect formation (e.g. internal cracks, pencil pipes, slivers and shell-thinning breakouts), which are closely associated with phenomena such as the transport of inclusions (e.g. alumina) and argon bubbles and heat transfer.

This flow has been extensively studied using the Reynolds averaged approach (mainly using the k-ε model) (Thomas and Zhang, 2001). However these models only predict the mean values but cannot capture the flow transients. LES

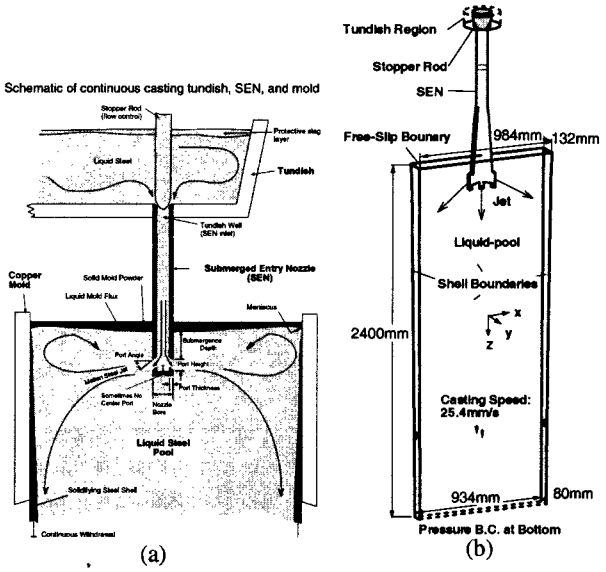


Figure 1. Schematics of (a) the continuous casting process and (b) the computational domain (*Case2-S*)

provides an attractive way to study this transient flow, in which the evolution and dynamics of large-scale eddies are resolved.

Compared to the extensive fundamental studies of LES on model turbulence problems (Kaltenbach, et al., 1999; Hughes, et al., 2001), its application to continuous casting is recent and rare (Sivaramakrishnan, et al., 2000; Yuan, et al., 2001; Takatani, et al., 2001). The difficulty lies in the following aspects: prescription of the transient inlet velocities, resolution of the complex domain geometry, moving solidifying front and long-term transients. To reduce the computational cost, previous published work either employs a coarse grid (Takatani, et al., 2001) or only models half of the liquid-pool (Sivaramakrishnan, et al., 2000; Yuan, et al., 2001) by assuming a symmetrical flow in the left and right halves (Fig. 1). Further, these simulations were mainly on scaled water models where measurements were available.

Physical water models have been widely used as an experimental tool to study flow in the liquid-pool of continuous cast steel, because of the nearly equal kinematic viscosities of water (at room temperature) and molten steel.

Compared to the steel caster, the water model allows flow visualization and accurate measurements (e.g. PIV). Although valuable, its difference from the steel caster should still be noted in two major aspects, which are important to the flow field. First, its sidewalls, which represent the moving solidifying shell front, are non-porous and stationary. The solidification effects on the flow are not modeled. Further, the water model has a flat bottom with outlet ports instead of the deep tapering molten steel pool. These two major differences cause different flow phenomena, which are investigated in this work.

The objective of this work is to understand the instantaneous flow structures in the steel caster, and to quantify the difference between the caster and the water model. Three LES computations are presented in this paper, where fine grids and more realistic domain geometries are employed, which are introduced in the following sections.

## PROBLEM DESCRIPTION

Table 1 presents parameters for three simulations named *Case 1*, *Case 2-W* and *Case 2-S* respectively. The first simulation (*Case 1*) is on a 0.4-scale water model, where PIV data are available (Assar, et al., 2000; Sivaramakrishnan, 2000). Half of the liquid-pool was modeled by imposing symmetry conditions at the center plane. The domain was discretized into a structured grid of 1.5 million cells. The unsteady inlet velocities are obtained from an LES nozzle simulation, collecting data at the port outlet plane every 0.01s for a period of 1.75s (Thomas and Vanka, 2001). The 1.75s velocities were then recycled periodically to serve as the inlet boundary condition. The comparison of this simulation with the PIV measurements is presented in the results section.

After comparing with PIV, LES was then applied to a real steel caster (*Case 2-S*) and its corresponding water model (*Case 2-W*). More realistic domain geometries were resolved for both cases by modeling the full liquid-pool. The computational domains were discretized into unstructured grids consisting of 1.3 and 0.75 million cells respectively. *Case 2-S* differs from *2-W* in two respects. Firstly a curved moving side boundary shown in Fig. 1(b) was used in *Case 2-S* to represent the downward moving solidification front, whereas the side wall for *Case 2-W* is straight and stationary. Secondly, solidification effects were modeled in *Case 2-S* by imposing a normal velocity at the side boundary. Both cases employ a constant pressure at the bottom boundary, which is far from the inlet. The top surface was modeled as a free-slip boundary. The transient inlet velocities were again collected from a nozzle simulation every 0.025s for 9.75s and recycled periodically.

## MATHEMATICAL MODELING

The unsteady three-dimensional Navier-Stokes equations were solved for the flow in the liquid pool during continuous casting:

Table 1: Properties and conditions of the simulations.

| Parameter/Property | *Case 1* | *Case 2-W* | *Case 2-S* |
|---|---|---|---|
| Mold width (mm) | 735 | 984 | 984 |
| Mold thickness (mm) | 95(top) 65(bottom) | 132 | 132 |
| Water model length (mm) | 950 | 2600 | - |
| Mold length (mm) | - | - | 1200 |
| Domain width (mm) | 367.5 | 984 | 984 (top) 934(bottom) |
| Domain thickness (mm) | 80 | 132 | 132 (top) 79.48 (bottom) |
| Domain length (mm) | 950 | 1200 | 2400 |
| SEN bore diameter (mm) | 32 | - | - |
| Nozzle port height × width (mm × mm) | 31(diameter) | 75 × 32 | 75 × 32 |
| Port thickness (mm) | 11 | 17.5 | 17.5 |
| Port angle, upper edge | 15° down | 15° down | 15° down |
| Port angle, lower angle | 40° down | 15° down | 15° down |
| Bottom port diameter (mm) | - | 32 | 32 |
| SEN submergence depth (mm) | 75 | 127 | 127 |
| Casting speed (mm/s) | 12.1 | 25.4 | 25.4 |
| Kinematic viscosity ($m^2/s$) | $1.0 \times 10^{-6}$ | $1.0 \times 10^{-6}$ | $7.98 \times 10^{-7}$ |

$$\frac{\partial v_i}{\partial x_i} = 0 \qquad [1]$$

$$\frac{Dv_i}{Dx_i} = -\frac{1}{\rho}\frac{\partial p}{\partial x_i} + \frac{\partial}{\partial x_j}\nu_{eff}\left(\frac{\partial v_i}{\partial x_j} + \frac{\partial v_j}{\partial x_i}\right) \qquad [2]$$

where the velocities are filtered values. Because of the relatively fine grids, no SGS models were employed, so these simulations can also be called coarse grid DNS.

The time-dependent three-dimensional Navier-Stokes equations were solved using the Harlow-Welch fractional step procedure. Second order central differencing is used for the convection terms and the Crank-Nicolson scheme is used for the diffusion terms. The Adams-Bashforth scheme is used to discretize in time with second order accuracy. The pressure Poisson equation is solved using a direct Fast Fourier Transform (FFT) solver for the first simulation and an Algebraic Multi-grid (AMG) solver for the last two simulations, depending on whether a structured or unstructured grid is used. The time step for all the simulations is 0.001s. The simulation took 29.5 CPU seconds per time step on a Pentium IV 1.7GHz PC for the 1.3 million cells grid or 24 days for 70,000 time steps (70s of real time) with the AMG solver. The FFT solver is about four times faster and takes about one quarter of the memory.

## RESULTS AND DISCUSSION

### Case 1

Figure 2 shows a typical instantaneous velocity vector plot at the plane y=0 (half way between wide faces, see Fig.1) obtained from LES and the PIV measurements on the 0.4-scale water model. Both plots show a double-recirculation flow pattern above and below the slant inflow jet. Chaotic

vortex structures can be seen in both the upper and lower recirculation zones, which evolve with time. The comparison shows that LES captures the main features of the flow. The computed velocity field is then averaged over 45s to compare with the PIV on the mean and *rms* values in Figs. 3 and 4 respectively.

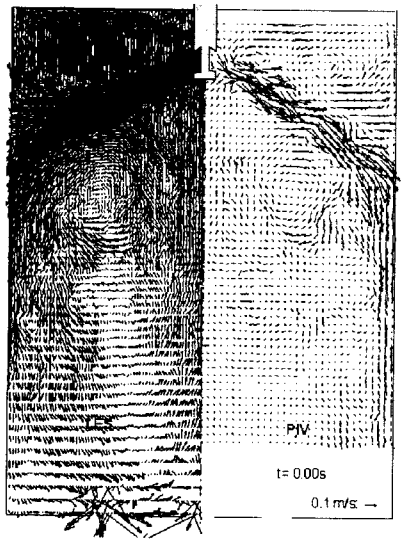


Figure 2. Instantaneous velocity vectors at the center plane.

Figure 3 shows the time-averaged horizontal velocity towards SEN along the top surface center line in the x direction (see Fig. 1). Due to the lack of PIV data on the top surface for the same casting speed, the LES is compared with two other measurements for slightly higher and lower casting speeds. It should be remarked that the PIV data in the figure are the average of several measurements. In both the measurements and the simulation, the horizontal velocity increases from the SEN, reaches its maximum half way between the SEN and the narrow face and then decreases approaching the narrow face. The quantitative comparison shows that the computation well agrees with the PIV data.

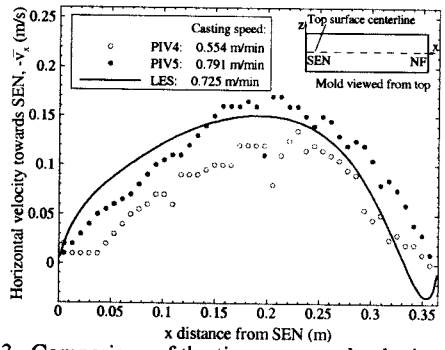


Figure 3. Comparison of the time-averaged velocity along the top surface centerline between LES and PIV (*Case 1*).

Figure 4 compares the computed *rms* velocities with the PIV measurements in the lower recirculation zone, where sufficient measurement data are available at the same casting speed. The data shown in the figure are *rms* of the vertical velocity component ($v_z$) along a horizontal line located in the plane y=0 and 0.5m below the top surface. The PIV data are averaged over 2000s (2000 frames). A significant asymmetry can be observed between the left and right half, suggesting the existence of a long-term asymmetry in the lower recirculation zone. The computation favorably matches the measurement of the left half, indicating the capacity of LES to accurately predict the second moments.

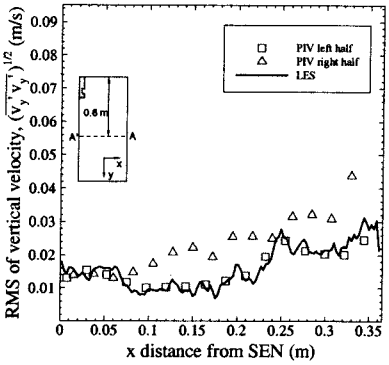


Figure 4. *rms* of the downward velocity along a line 0.5m below the top surface, obtained from LES and PIV (*Case 1*).

The comparison of LES and PIV on the 0.4-scale water model suggests that the LES predicts the velocity field with a reasonable accuracy. It also shows the importance of modeling the full liquid-pool domain, in order to quantify long-term asymmetries.

## Velocity Field in the Liquid-Pool (*Cases 2-S & 2-W*)

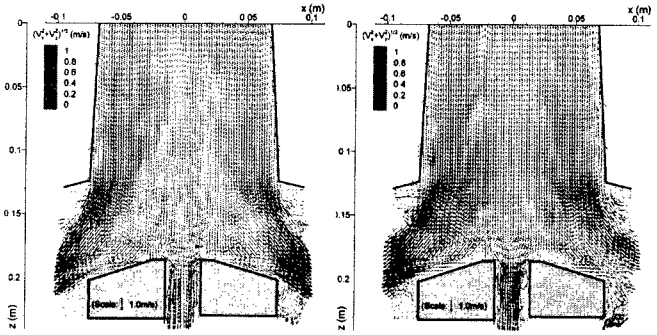

Figure 5. Instantaneous velocities leaving nozzle ports.

As mentioned before, a nozzle simulation was conducted to generate unsteady inlet velocities for *Cases 2-S* and *2-W*. Figure 7 presents two typical instantaneous plots of the velocity near the SEN ports at the plane y=0. In contrast to the left plot, which reveals a fairly symmetrical flow field, the right plot shows a deeper jet angle leaving the left port. The downward jet angle varies from ~30° to ~45° in the simulation. Both patterns persist for only a short time and switch between each other. The jet angle is important to the flow in the liquid-pool. This angle influences the removal of harmful inclusions/bubbles carried by the jet into the liquid-pool. It also affects the velocity and liquid level across the

top surface. Generally, deep angled jets tend to transport more inclusions into the lower zone, encouraging the formation of internal defects (e.g. slivers and blisters). Shallow jet angles likely cause a high top surface velocity and level fluctuations, which can cause surface defects and slag entrainment. Accurate prediction of the jet angle is important to liquid-pool simulations and permits action of optimizing the nozzle design.

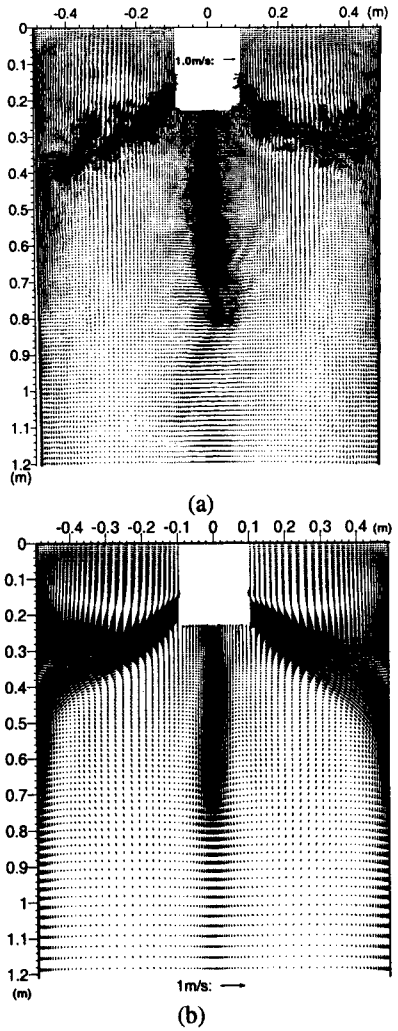


Figure 6. Predicted (a) instantaneous and (b) time-averaged velocity plots at y=0 (*Case 2-S*).

The computed velocity field in the liquid-pool is shown in Fig. 6 at the plane y=0 (*Case 2-S*). The upper plot presents an instantaneous velocity field and the lower shows the time-average over 51s. A qualitatively similar velocity field is obtained for *Case 2-W* but is not shown here. The double roll flow pattern is observed in both plots. Compared with the dye-injection on the same water model (Yuan, et al., 2003), the predicted jet shape and the location of the upper and lower rolls match the experiment favorably. Different from the smooth time-averaged plot, the instantaneous velocity plot shows chaotic local turbulent structures evolving with time, which is similar to *Case 1*. The center jet is seen to oscillate in the simulation, which is again consistent with the dye injection. In the time-averaged plot, a slight asymmetry exists in the center jet. For both cases the time-average was taken for approximately 50s. This asymmetry indicates that the center jet oscillation has a low-frequency component, which might lead to transient asymmetrical defects that are observed in plants.

## Comparison of Steel Casters and Water Models (*Case 2-S* vs. *2-W*)

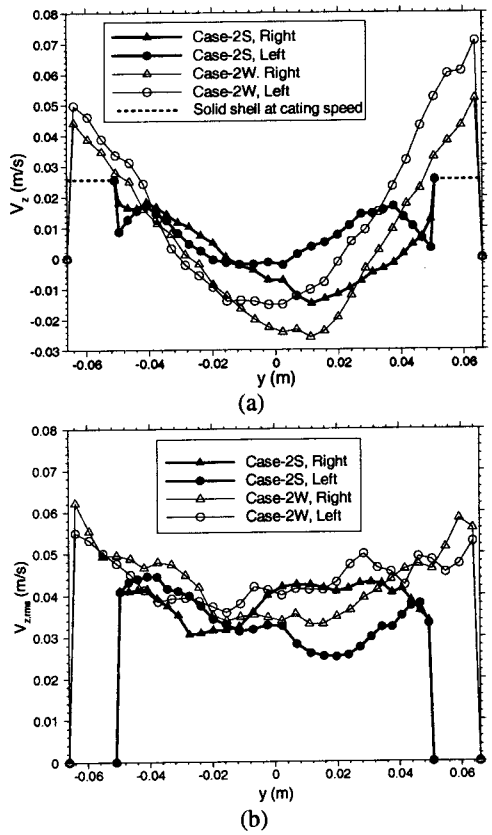


Figure 7. Comparison of (a) the mean and (b) the *rms* values of the downward velocity between *Case 2-S* and *Case 2-W*.

Figures 7(a) and (b) compare the steel caster (*Case 2-S*) and the corresponding water model (*Case 2-W*) with the mean and *rms* values of the downward velocity ($v_z$). The data are obtained along a horizontal line 1000mm below the top surface and 164mm from the narrow face. A bigger spatial variation of the averaged velocity is seen for the water model (Fig. 7(a)). The figure also shows that the steel caster has less upward (or reverse) flow. Two reasons are suspected to cause this: the tapering and solidification restricts the flow domain, which hastens the even distribution of the flow; and the downward withdrawal of the shell discourages the flow to have upward motion. An asymmetry between the two sides can also be seen for both cases, implying the existence of a low frequency oscillation between the two sides with a period longer than the averaging time (~50s).

## Flow Asymmetries

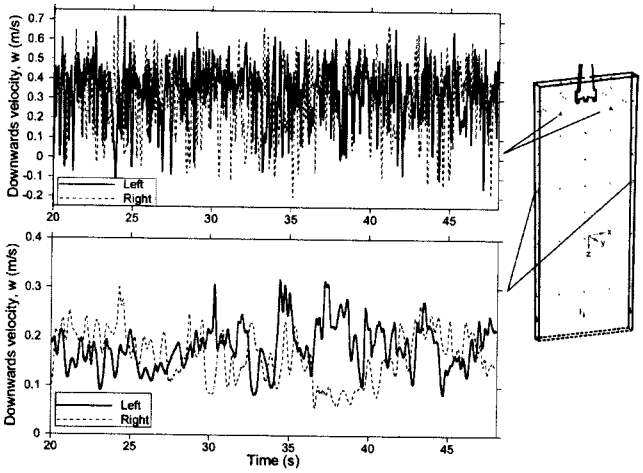


Figure 8. Time variations of downward velocity at two pairs of symmetrical points (*Case 2-S*).

The flow asymmetry is further investigated in Fig. 8, which shows the time-variation of the downward velocity at two pairs of monitoring points, each symmetrically located in the liquid-pool (as shown in the figure). The data are collected every 0.001s in the simulation of *Case 2-S*. The first pair of points (solid triangles) is located in the middle of the jet. The other pair is 1.2m below the top surface and near the narrow face. The upper plot presents the velocity history of first pair of points, showing high-frequency fluctuations. The lower plot, which presents the velocity history of the second pair of points, clearly shows a significant long-term asymmetry (e.g. from 37s to 40s), which repeats at a lower frequency in the simulation. These observations suggest that (1) low frequency long-term asymmetries exist in the lower recirculation zone; (2) the asymmetries are due to the nature of turbulence rather than imposed by the inlet jet. This finding is important to understanding the behavior of inclusion particles. Particles transported to a deeper location are more likely to become permanently entrapped in the steel caster and form intermittent and asymmetrical defects.

## Top Surface Velocity and Liquid Level

Figure 9(a) shows the time-variation of the horizontal velocity towards the SEN obtained from the simulation of *Case 2-S*. The data are taken at the center point of the top surface (in the middle between the SEN and the narrow face). The velocity fluctuations are large – comparable in magnitude to the local time-averaged values. Figure 9 (a) shows a large velocity component with high frequency (e.g. the velocity drops from ~0.4m/s towards the SEN to a velocity in the opposite direction within 0.2s). Due to the lack of long-term measurements of unsteady velocities in this caster (*Case 2-S*) as well as in the corresponding water model (*Case 2-W*), this result is compared with the PIV measurements in the 0.4-scale water model (*Case 1*), which is presented in Fig. 9(b). A similar velocity behavior, as observed in *Case 2-S*, is also seen in the PIV measurements. Neither LES simulation in Fig 9(b) captures the measured behavior, where symmetrical flow is assumed for each half of the liquid-pool. This suggests that interaction between the two halves of the caster is the cause of large high frequency fluctuations. It also suggests that some important transient flow phenomena will be inherently missed in half-domain simulations because the symmetry assumption is imposed. This velocity variation is important, because the liquid level fluctuations accompanying it are a major cause of defects in the process.

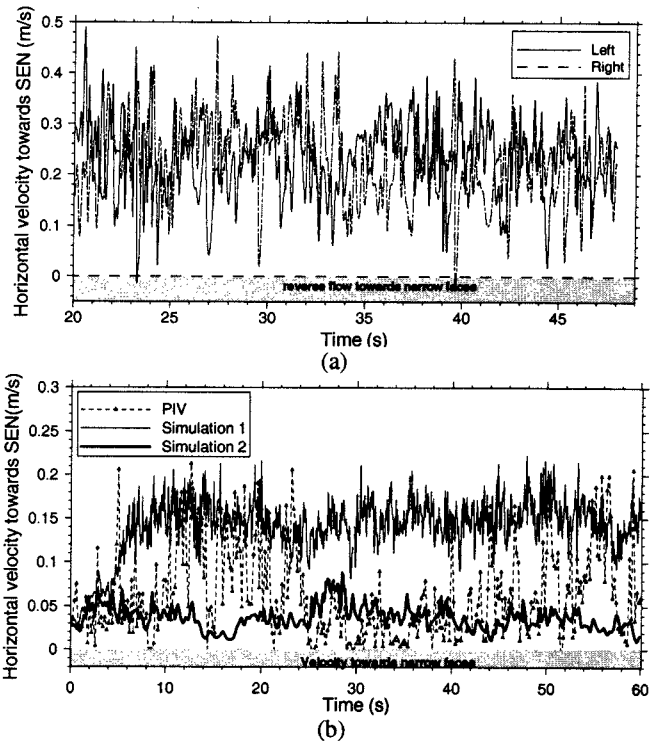


Figure 9. Time variations of the horizontal velocity towards SEN at the center point of the top surface: (a) *Case 2-S* and (b) the 0.4-scale water model.

Liquid level across the top surface is an important parameter for continuous casting. The level changes the local thickness of the flux layer, which covers the molten steel on the top to prevent re-oxidation (see Fig. 1). This flux layer needs to be thick enough in order to provide a steady supply of molten flux into the interfacial gap between the mold and the shell to lubricate the steel. Insufficient flux consumption leads to temperature fluctuations which cause surface cracks and other defects in the solid steel product. The dynamic mesh is one method to accurately predict this level but this will dramatically increases the computational cost. In this work where static meshes are employed, the liquid level is estimated based on the computed pressure across the top surface by:

$$h = \frac{(p - p_{mean})}{(\rho_{steel} - \rho_{flux})g} \qquad [3]$$

Figure 10(a) shows the water model (*Case 2-W*) prediction compared with the measured levels on video at three instants. Figure 10(b) presents the predicted molten steel level at the top surface together with industry measurements using nail sheets. Uncertainty in the measurement exists regarding possible rotation of the aluminum sheets used in the measurements. For both cases, the level is higher near the narrow face by 2mm (water model) and 4-6mm (steel caster). The steel fluctuations are greater because the steel upward momentum near the narrow face lifts the liquid level there, displacing some of the molten flux. Both the predictions agree with the measurements within their uncertainty.

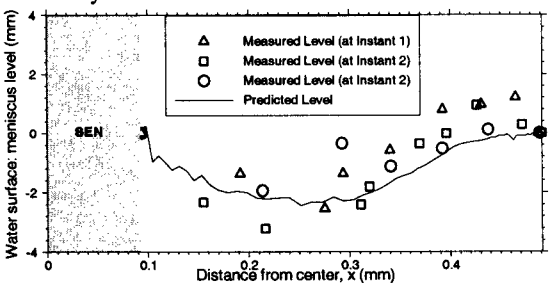


(a)

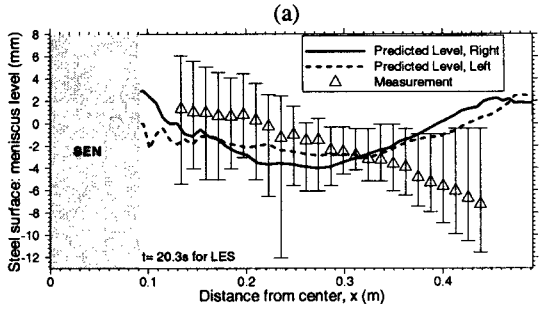


(b)

Figure 10. Comparison of predicted and measured top surface liquid levels in: (a) *Case 2-W* and (b) *Case 2-S*.

## CONCLUSIONS

This work shows that in a continuous caster LES is capable of predicting the mean and *rms* velocities with a good accuracy. It also shows that LES captures the transient flow features compared with experiments (Figs. 2, 6 and 9). Transient asymmetries are found both across the top surface and in the lower recirculation zone to be an important feature of the flow in the liquid pool. Interaction between the two halves is found to be an important cause of the asymmetries. Half-pool simulations inherently miss the asymmetry and the consequent oscillations. Water models are generally representative of steel casters, especially near the top surface. However, steel casters are likely to have more evenly distributed downward flow in the lower recirculation zone. This work also suggests that low-amplitude variations of the top surface liquid level can be reasonably estimated based on the pressure distribution.


## ACKNOWLEDGEMENTS

The authors thank the National Science Foundation (Grant DMI-01-15486) which made this research possible. The work is also supported by the member companies of the Continuous Casting Consortium at University of Illinois at Urbana-Champaign (UIUC). Special thanks are due to Ya Meng for calculating the shell thickness and the National Center for Supercomputing Applications (NCSA) at UIUC for computational facilities.


## REFERENCES:


Thomas, B. G. and L. Zhang, *Mathematical Modeling of Fluid Flow in Continuous Casting*. ISIJ International,2001, **41**(10): p. 1181-1193.

Kaltenbach, H.-J., M. Fatica, R. Mittal, T.S. Lund, and P. Moin, *Study of Flow in a Planar Asymmetric Diffuser using Large-Eddy Simulation.* Journal of Fluid Mechanics, 1999. **390**: p. 151-185.

Hughes, T.J.R., A.A. Oberai, and L. Mazzei, *Large Eddy Simulation of Turbulent Channel Flows by the Variational Multiscale Method.* Physics of Fluids, 2001. **13**(6): p. 1784-1799.

Sivaramakrishnan, S., H. Bai, B.G. Thomas, P. Vanka, P. Dauby, and M. Assar, *Transient Flow Structures in Continuous Cast Steel,* in *Ironmaking Conference Proceedings*. 2000, ISS, Warrendale, PA p. 541-557.

Yuan, Q., S. P. Vanka and B. G. Thomas, *Large Eddy Simulations of Turbulent Flow and Inclusion Transport in Continuous Casting of Steel.* TSFP2, June 27-29, 2001, Royal Insitute of Technology, Stockholm, Sweden.

Takatani, K., Y. Tanizawa, Hideo Mizukami, Kenzi Nishimura, *Mathematical Model for Transient Fluid Flow in a Continuous Casting Mold.* ISIJ International,2001, **41**(10): p. 1252-1261.

Assar, M. B., P. H. Dauby and G.D. Lawson, *Opening the Black Box: PIV and MFC Measurements in a Continuous Caster Mold.* Steelmaking Conference Proceedings, ISS, Warrendale, PA. 2000, **83:** 397-411.

Sivaramakrishnan, S. *Transient Fluid Flow in the Mold and Heat Transfer Through the Molten Slag Layer in Continuous Casting of Steel*, University of Illinois, Master Thesis, 2000.

Thomas, B. G. and S. P. Vanka, *Study of Transient Flow Structures in the Continuous Casting of Steel.* NSF Design & Manufacturing Grantees Conference, Jan. 7-10, 2001, Tampa, FL, NSF, Washington, D.C.

Yuan, Q., B. G. Thomas and S.P. Vanka. *Turbulent Flow and Particle Motion in Continuous Slab-Casting.* ISSTech 2003, April 27 - 30, 2003, Indianapolis, IN, USA.